ORIGINAL PAPER

A Novel Wave Reflection Model of the Human Arterial System

Hongjun Zhang · John K-J. Li

Abstract A frequency domain distributed 55 segment arterial model was constructed from the reflection perspective to predict pressure waveforms in the large systemic arteries. At any node, the predicted pressure waveform was the combination of a forward propagating waveform and a number of repeatedly reflected waveforms from any possible sites. This approach ensured that any single reflected waveform could be traced back to its origin, and thus the causal-effect relation would be precisely known. This model was evaluated in terms of branch reflection coefficient, terminal vascular bed behavior, and wall viscoelasticity. It was found that the model predicted pressure waveforms were most sensitive to the branch reflection coefficient, and this led to the adoption of the zero-forward reflection assumption at branches. The model-predicted pressure waveforms compared favorably with realistic blood pressure waveforms, especially in the upper limbs. For lower limbs, finer segmentation could further improve the predictions.

Keywords Arterial hemodynamics · Distributed model · Blood pressure waveforms · Pulse wave propagation · Pulse wave reflection

H. Zhang (✉) · J. K-J. Li
Biomedical Engineering, Rutgers University, 599 Taylor Road, BME, Piscataway, NJ 08854, USA
e-mail: hongjun@rci.rutgers.edu

J. K-J. Li
e-mail: johnkjli@rci.rutgers.edu

Introduction

The amplification of pressure pulses as a result of reflections in the periphery was first identified in nineteenth century by Spengler and Von Kries (Li 2000). The amplification of pressure pulses has been attributed to the in-phase summation of reflected waves arising from structural and geometric non-uniformities. The arteriolar beds have been recognized as the principal reflection sites. Thus, pulsatile pressure and flow waveforms contain information about the heart as well as the vascular system.

The study of pulse waveform contours is important, because of its relevance to many cardiovascular diseases. Alterations in contours are closely related to the mechanical properties of the vessel wall and vascular states, and are linked to hypertension and atherosclerosis (O'Rourke 1970; Safar et al. 1984). In hypertension, for instance, the increased pressure is always associated with increased wave reflections (Li 1989). Increased wave reflections impede ejection and are detrimental to normal LV function. This increased wave reflection can occur as a consequence of changing vascular bed characteristics or the modification of conduit vessel wall properties.

Due to the lack of means for direct measurement of the timing, amplitude and sites of wave reflection and complexity of the nature of wave reflection, model study emerges as an important tool. There are numerous models of the arterial system; some are linear models based on transmission line theories (e.g. Noordergraaf et al. 1963; Westerhof et al. 1969; Avolio 1980) others are nonlinear models (Snyder et al. 1968; Stergiopulos et al. 1992). Few models utilize reflection phenomena sufficiently and directly. A propagating pulse wave is traceable. And its resultant waveform at any location can be ascribed to individual reflected waves so that a causal relation can be

established to describe the relationships between different sites of interests (Berger et al. 1993). A recent model proposed by Wang and Parker (2004) dealt with reflection directly in the time domain. But viscosity was neglected in the model, therefore wall-damping effects were underestimated. Also, their model did not compare with actual measured data.

We present here a model of the arterial system from a new perspective that emphasizes wave reflection directly, intuitively, and thoroughly. The main difference between this model and the traditional transmission models lies in how reflection is treated and that the predicted pressure waveform becomes the combination of a forward propagating waveform and a number of repeatedly reflected waveforms from many possible sites. This approach ensured that any single reflected waveform could be traced back to its origin, and thus the causal-effect relation would be precisely known.

Methods

The construction of the proposed arterial model consists of three steps: single segment modeling, interaction between segments, and multi-segment network connections.

Pulsatile Wave Propagation in a Single Segment

The basic computational unit is a segment of artery which is a thin-walled cylindrical tube having internal viscous, elastic and inertial properties with external coupling to the surrounding tissue producing a longitudinal constraint (Avolio 1980). The transmission ratio of pressure at the one end p_2 to pressure at the other end of a segment $p_1 = A_1 e^{j\omega t}$ for a certain frequency ω is given by Taylor (1966) if assuming no reflection occurs.

$$p_2 = p_1 e^{-\gamma l} = A_1 e^{j\omega t} e^{-\gamma l} \tag{1}$$

where l is the length of the segment, and γ is the propagation constant. The above equation applies to transmission that occurs in either direction. The propagation constant describes the transmission of sinusoidal waves with respect to the spatial change of phase (phase coefficient β) and the spatial decrease in amplitude (damping or attenuation coefficient α)

$$\gamma = \frac{j\omega}{c_{ph}} = \alpha + j\beta \tag{2}$$

where c_{ph} is the complex phase velocity. c_{ph} was calculated from Womersley's analysis for a uniform tube, and is a function of viscous blood flow, viscoelasticity of the vessel wall, Poisson ratio of the wall material, and the external constraints on wall motion. Womersley (1957)

$$c_{ph} = \frac{c_0}{(X - jY)(1 - j\omega W)} \tag{3}$$

c_0 is the pulse wave velocity defined by the Moens-Korteweg equation

$$c_0 = \sqrt{\frac{Eh}{\rho D}} \tag{4}$$

where h is the arterial wall thickness, D is the internal diameter, and ρ is blood density taken as 1.05 gm/cm³. E is the static Young's modulus of the arterial wall. The arterial wall behaves as a viscoelastic material that produces a phase difference ϕ between applied force and resulting displacement (Taylor 1966). The term $(1 - j\omega t)$ in Eq. 3 takes into account the effects of wall viscosity:

$$(1 - j\omega W) = 1 - j\frac{\tan \phi}{2} \cong e^{-j\phi/2} \tag{5}$$

and the above approximation is based upon the fact that ϕ is small for aorta (Bergel 1961), where the angle ϕ is expressed in terms of wall viscosity η

$$\phi = \tan^{-1}\left(\frac{\omega\eta}{E}\right) \tag{6}$$

Taylor (1966) derived an expression for the variation of ϕ with frequency as

$$\phi = \phi_0(1 - e^{-k\omega}) \tag{7}$$

where ϕ_0 is an asymptotic value that was taken as 15° by Avolio (1980) and k was taken as 2. Karamanoglu et al. (1995) observed a relationship for ϕ_0

$$\phi_0 \cong \phi(10h/2r) \tag{8}$$

where $h/2r$ is the wall thickness to diameter ratio, and φ is taken 5°, 10° and 15°. Since minimal effects were obtained using different φ, $\varphi = 10°$ is used in this study to obtain ϕ.

The term $(X - jY)$ in Eq. 3 takes into account the effects of blood viscosity and longitudinal constraint:

$$(X - jY)|_{k=-\infty} = \frac{\sqrt{(1 - \sigma^2)}}{\sqrt{(1 - F_{10})}} \tag{9}$$

where σ is Poisson's ratio and is taken as 0.5; k is a variable which expresses the longitudinal constraint and loading ($k = -\infty$) is a condition of maximal constraint and loading). The complex function $(1 - F_{10})$ may be expressed in modulus (M'_{10}) and phase (ε'_{10})

$$(1 - F_{10}) = M'_{10} e^{j\varepsilon'_{10}} \tag{10}$$

Womersley (1957) tabulated the modulus and phase for various values of σ_ω, where σ_ω is the non-dimensional Womersley's parameter

$$\alpha_\omega = r\sqrt{\frac{\omega\rho}{\mu}} \tag{11}$$

where μ is the blood viscosity (0.04 poise), and r is the internal arterial radius. Substituting Eqs. 5, 9, and 10 into Eq. 3, and solving for c_{ph} yields

$$c_{ph} = \frac{c_0 (M'_{10})^{1/2} e^{j\varepsilon'_{10}/2} e^{j\phi/2}}{(1-\sigma^2)^{1/2}} \tag{12}$$

Substitute Eq. 12 into Eq. 2 and we obtain

$$\gamma = \frac{\omega(1-\sigma^2)^{1/2}}{c_0 (M'_{10})^{1/2}} \left[\sin\left(\frac{\varepsilon'_{10}+\phi}{2}\right) + j\cos\left(\frac{\varepsilon'_{10}+\phi}{2}\right) \right] \tag{13}$$

attenuation coefficient:

$$\alpha = \frac{\omega(1-\sigma^2)^{1/2}}{c_0 (M'_{10})^{1/2}} \sin\left(\frac{\varepsilon'_{10}+\phi}{2}\right) \tag{14}$$

phase coefficient:

$$\beta = \frac{\omega(1-\sigma^2)^{1/2}}{c_0 (M'_{10})^{1/2}} \cos\left(\frac{\varepsilon'_{10}+\phi}{2}\right) \tag{15}$$

Inter-Segmental Interaction

Characteristic Impedance

The characteristic impedance of an arterial segment as derived by Womersley (1957) is

$$Z_o = \frac{\rho c_0}{\pi r^2 \sqrt{1-\sigma^2}} (1 - F_{10})^{-1/2} \tag{16}$$

In this expression, Z_o is a function of blood viscosity and oscillatory frequency, and longitudinal constraint and loading is allowed for. With inclusion of wall viscosity, we have:

$$Z_o = \frac{\rho c_o}{\pi r^2 (1-\sigma^2)^{1/2} (1-F_{10})^{1/2} (1-j\omega W)} \tag{17}$$

Z_o can also be calculated with the water hammer equation (Li 1987, 2004):

$$Z_o = \frac{\rho c_0}{\pi r^2} \tag{18}$$

In this expression, Z_o only represents the local geometry. Eq. 18 can be approximated from Eq. 17 by assuming infinite σ_ω. The difference in using the two expressions in calculating local reflection coefficient with respect to branch area ratio is shown to be small in major arteries (Noordergraaf 1969). Therefore, for simplicity, Eq. 18 is used to calculate the characteristic impedance.

Reflection at Bifurcations

Wave reflections occur from any discontinuity along the arterial tree, and possible reflecting sites are branching points, areas of alteration in arterial distensibility (geometric and elastic tapering), and high resistance terminal beds. Consider at a bifurcation, a wave traveling down the parent segment will be partially reflected at the junction and partially transmitted to the daughter segments. The relationship between the incident, reflected and transmitted waves is determined by the conditions of one-dimensional flow at junctions (Wang 1997): (1) the mass must be conserved and (2) the pressure is continuous across the junction. For pressure, this relationship is expressed as

$$\Delta P_0 + dP_0 = dP_1 = dP_2 \tag{19}$$

where ΔP_0 is the incident pressure in the parent segment at the junction, dP_0 is the reflected portion in the parent segment at the junction, and dP_1 and dP_2 are the transmitted portion in the daughter segments at the junction.

The reflection coefficient can be derived from the above two conditions as

$$\Gamma_B = \frac{Z_o^{-1} - Z_1^{-1} - Z_2^{-1}}{Z_o^{-1} + Z_1^{-1} + Z_2^{-1}} \tag{20}$$

where Z_o is the characteristic impedance of the parent segment; in traditional transmission line models, Z_1 and Z_2 are the input impedances of the two daughter segments (Li et al. 1984), and they represent the impedance that can be 'seen' from the bifurcating point on to all downstream (with respect to the propagation direction) vascular branches. This approach was also used by Wang and Parker (2004). This equation also applies when the wave travels backward. Therefore, the parent and daughter segments are defined with respect to wave traveling direction (Li et al. 1984).

The transmission coefficient T is given by

$$T = 1 + \Gamma_B \tag{21}$$

The forward reflection coefficients have been experimentally shown to be small for major arterial branches (Hardung 1952; Gosling et al. 1971; Li et al. 1984, 1986b; Papageorgiou et al. 1990). The backward or retrograde reflections at branches are large (Li et al. 1984).

Reflection at Terminal Beds and Terminal Impedance Modeling

The high impedance arterioles have been agreed to be the major sites of pulse wave reflection (McDonald 1974; Li 1987). Two approaches can be used to model the lumped terminal impedance. One is to model it as a pure resistance. The other is to model it with a modified Windkessel as in

Stergiopulos ([1990](#)). We modeled both and the differences were not found significant which implies that terminal beds are primarily resistive. The values of total terminal resistances Rt used in this study are obtained from Schaaf and Abbrecht ([1972](#)). The terminal reflection coefficient is given by

$$\Gamma_T = \frac{R_t - Z_o}{R_t + Z_o} \tag{22}$$

Arterial Tree and Physiological Data

A schematic representation of the arterial tree used in this study is shown in Fig. [1](#). A common source of physiology data of the arterial tree used in many models (Westerhof et al. [1969](#); Schaaf and Abbrecht [1972](#); Avolio [1980](#); Stergiopulos et al. [1992](#); Wang and Parker [2004](#)) was complied by Noordergraaf et al. ([1963](#)) and subsequently modified by Westerhof et al. ([1969](#)). The arterial model of this study is based upon Stergiopulos's version ([1990](#)) of data that has 55 segments. Whenever an ambiguity arises, it is tracked back to Westerhof et al.'s data ([1969](#)) that has 121 segments. It would be more accurate to have 121 segments to reflect geometric and elastic tapering. However, due to the consideration of computation time, 58 segments are adopted in this study with 3 more segments added to the original 55 segments as stenotic points. The geometric, elastic, and terminal resistance data presented below are considered representative of a healthy young adult.

Geometric Data

The geometric properties of an arterial segment include: length, proximal and distal radii, and wall thickness (h). The proximal and distal radii are used to calculate the reflection coefficients at the proximal and distal branches (or terminal bed). The mean radius is used to calculate propagation constant. Geometric tapering is included in segmentation. In general, the finer the segmentation is, the smaller the error.

Elastic Properties

Young's modulus of elasticity (static elasticity) is a function of both distending pressure and location (elastic tapering) along the arterial tree. The relationship between elasticity and distending pressure is non-linear and not considered in the current study. Elastic tapering is considered by the method used by Westerhof et al. ([1969](#)):

1. For the main arterial trunk, upper arms and legs, and lower part of the carotid artery, $E = 4 \times 10^6$ g cm^{-1} s^{-2},

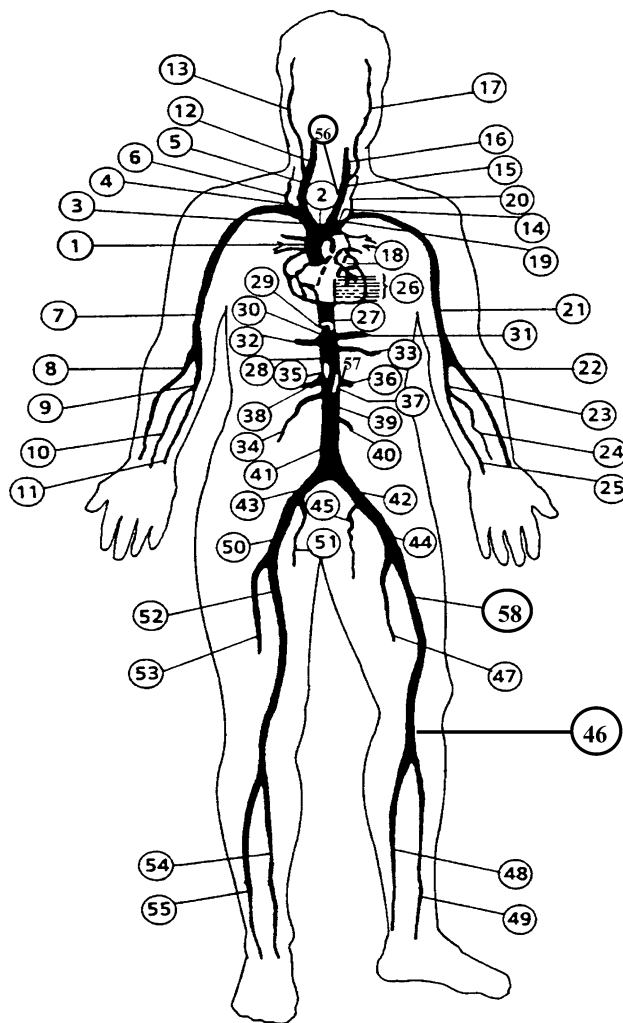**Fig. 1** Model of the human arterial system (from Stergiopulos [1990](#)). Three stenosis segments are added *46*, *56*, and *57*. Seg. *58* is used to designate the original seg. *46*

2. For the middle part of legs, arms, and head, $E = 8 \times 10^6$ g cm^{-1} s^{-2}, and
3. For the lower part of arms and legs, $E = 16 \times 10^6$ g cm^{-1} s^{-2}.

In Stergiopulos's arterial model ([1990](#)), the femoral artery is equivalent to the combination of the femoral artery ($l = 25.4$ cm, $E = 4 \times 10^6$ g cm^{-1} s^{-2}) and popliteal artery ($l = 18.9$ cm, $E = 8 \times 10^6$ g cm^{-1} s^{-2}) in Westerhof et al.'s model ([1969](#)). Therefore, an average value is taken as $E = 6 \times 10^6$ g cm^{-1} s^{-2}. Physiologic data is completed by assuming a Newtonian fluid with a constant dynamic viscosity $\mu = 0.0045$ N s m^{-2}.

Network Construction

Computation is carried out in a network that is defined in terms of branches, segments, and nodes. A detailed

description can be found in the Zhang (2006). The arterial model shown in Fig. 1 is translated into 30-branches/58-segments/116-nodes.

Within a segment, pressure wave propagation is determined by the propagation constant (Eq. 2) and not affected by the wave direction. When the 1st originating wave begins from 1st node of a segment and propagates toward the 2nd node of the same segment, it becomes a forward wave at the 2nd node; a reflected wave also occurs at the 2nd node; a transmitted (also forward) wave may occur also at the 1st node of the neighboring segment if it is a branch. Then the same pattern repeats in the neighboring segment till all segments are propagated by the 1st originating wave. Then each reflected wave acts as an originating wave and propagates the network again. Each reflected wave reaches different parts of the network according to the topology. This interaction pattern can be defined by an interaction distribution matrix described below.

Then according to this interaction distribution matrix, propagation (1st originating wave) starts from the heart (node 1) with unit amplitude and zero phases for a harmonic frequency, and propagates through the arterial tree, creating forward and reflected components at each node, by multiplying the propagation constants, transmission and reflection coefficients that apply. The propagation from the heart is the forward propagation that completes when all other nodes have been reached. Then, the reflected wave with unit amplitude and zero phase at node 2 acts like the heart and propagates throughout the arterial tree, generating forward and reflected components. The entire propagation process from node 1 to node 116 is called a (round of) propagation distribution for a harmonic frequency. Certainly, the repeated (secondary) reflections do not necessarily end when a round of propagation distribution completes. Reflections end only when all energy is dissipated by blood and arterial wall viscosity. The propagation distribution is described by a (232×116) complex number matrix (with amplitude and phase). There is one propagation distribution matrix for each harmonic frequency.

A multi-reflection matrix is the result of applying the propagation distribute matrix repeatedly until all energy is lost (implemented by a given threshold). Once the multi-reflection matrixes have been obtained for all harmonic frequencies, analysis can be performed to obtain simulated experimental results. For example, pressure waveform at the heart (node 1) can be obtained by adding up all corresponding components at all harmonic frequencies. Forward and reflected components can also be tracked separately.

Results

Model Evaluation

Forward Input Pressure Waveform

A forward input pressure waveform with fundamental frequency 1.17 Hz that corresponds to a heart rate of 70 beats/min and a cardiac period of 0.86 s. Systole occupies 40% and diastole, 60%, of the cardiac cycle. An amplitude threshold of 1% was given to control the convergence of simulation.

Branch Reflection Coefficient

Forward propagating waves encounter little reflections at vascular branches, i.e. vascular junction is pretty matched. For this reason, most branches can be assumed to have zero or a small forward reflection coefficient (below 0.20).

The calculated pressure waveforms for the original dimension and for modified dimension (Fig. 2) are compared against pressure waveforms from literature (e.g. Guyton 1976), where some characteristic features can be found (McDonald 1974; Li 2004): (1) Significant amplification of the pulse pressure along the arterial tree; (2) The incisura (dicrotic notch) is attenuated quickly resulting in a smoother waveform; (3) Peripheral pressure exhibits a secondary hump after the end of systole, due to reflection from proximity of a nearby vascular bed. It can be seen in Fig. 2 that the pulse pressure amplification is more evident for the zero forward reflection assumption and agrees well with Guyton's (1976) data.

The forward and reflected components at the aorta are also illustrated in Fig. 2. The reflection starts at about 100 ms after the beginning of systole for the zero forward reflection assumption, while about 40 ms for the original non-zero forward reflection case. Aortic reflection has generally been found to be very small in the early part of systole, i.e. the first 80 ms into systole is thought to be reflection-free (Li 1986a). In the elderly, aortic pressure exhibits early reflection, but it is related to stiffened arterial vessels (Li et al. 2007). And in this study, the data of the arterial model are assumed from a normal young adult.

Pressure Waveforms for the Control Case

A more complete set of pressure waveforms for the control case is shown in Fig. 3. The pressure waveform is decomposed into the forward and reflected components. Hemodynamic characteristics of the pressure waveforms are listed in Table 1.
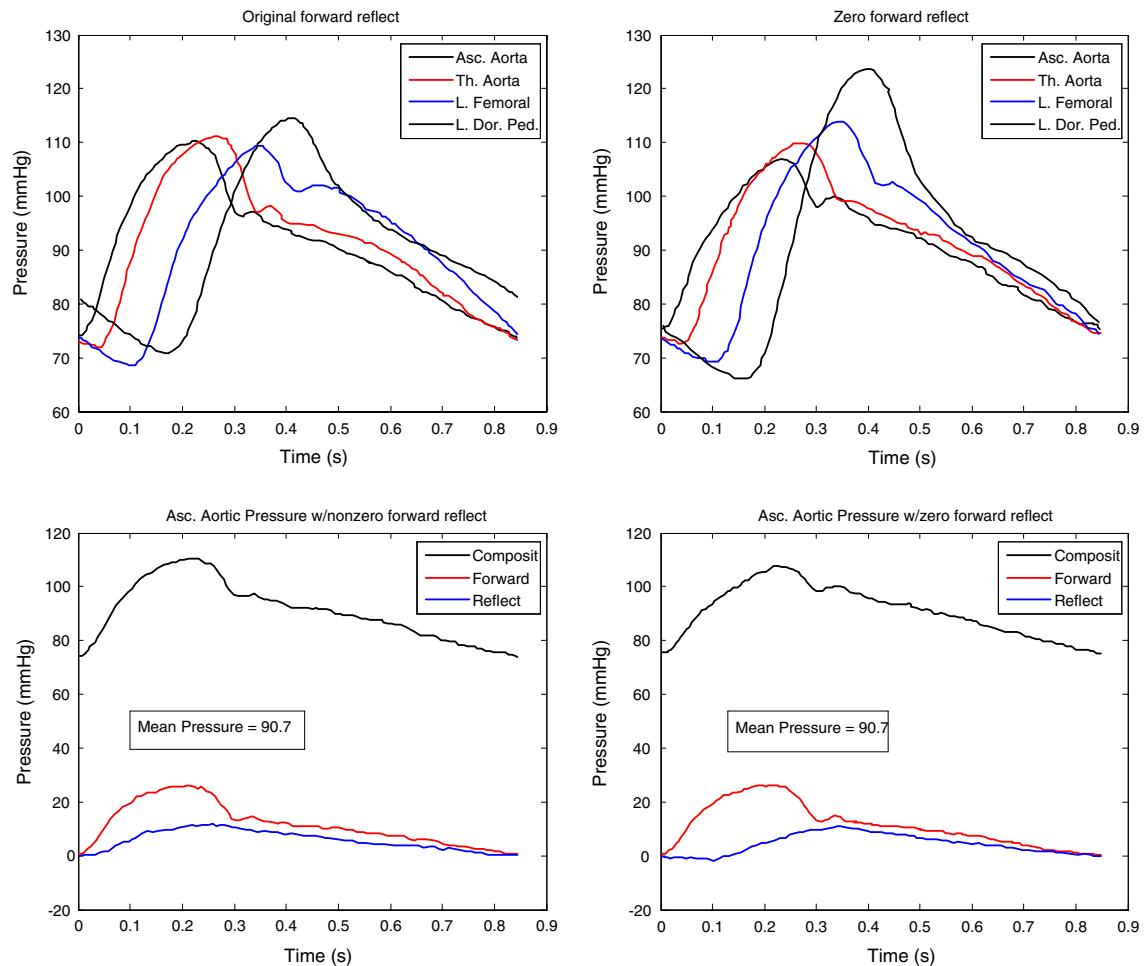
Fig. 2 *Upper left*: pressure waveforms with original forward reflection coefficients; *Upper right*: pressure waveforms with zero forward reflection coefficients; *Lower left*: asc. aortic pressure with original forward reflection and is decomposed into forward (input) and reflected components; *Lower left*: asc. aortic pressure with zero forward reflection and is decomposed into forward (input) and reflected components

From Fig. 3; Table 1, pulse pressure amplification is evident. Also the incisura becomes smoother, but does not disappear until after the femoral artery. The second hump basically is not seen in lower limbs. But the pressure waveforms in the brachial and radial arteries have evident second humps (diastolic waves) and the incisura is damped out. This preservation of the appearance of incisura and near absence of the second hump is attributed to fewer segments in the lower limbs. When the reflection travels backward or retrograde propagation, it is attenuated at branches because of the negative backward reflection coefficients. Therefore, fewer segments means that reflected waves can reach further up the arterial tree than the case of more segments, where reflections are very much confined to the local area. In addition, reflections have more effects on other adjacent branches in the case of fewer segments. Other features observed in Fig. 3; Table 1

are the attenuation in the forward components and accentuation in the reflected components.

Wall Viscosity

The wall viscosity was expressed as an angle φ, and $\varphi = 10°$ was used for the control case with wall viscosity, and $\varphi = 0$ for the non-viscosity case. Only the attenuation coefficients are affected by the wall viscosity. Neglecting the wall viscosity decreases the attenuation coefficients and increases pressure amplitudes.

The morphologic comparison between pressure waveforms with and without the wall viscosity is made in Fig. 4 (upper). For the ascending aorta, the difference is insignificant except for a minimally elevated diastolic. For the femoral artery, both the systolic and diastolic peaks increase and also much of the diastolic portion is increased

Fig. 3 Forward and reflected components for the control case
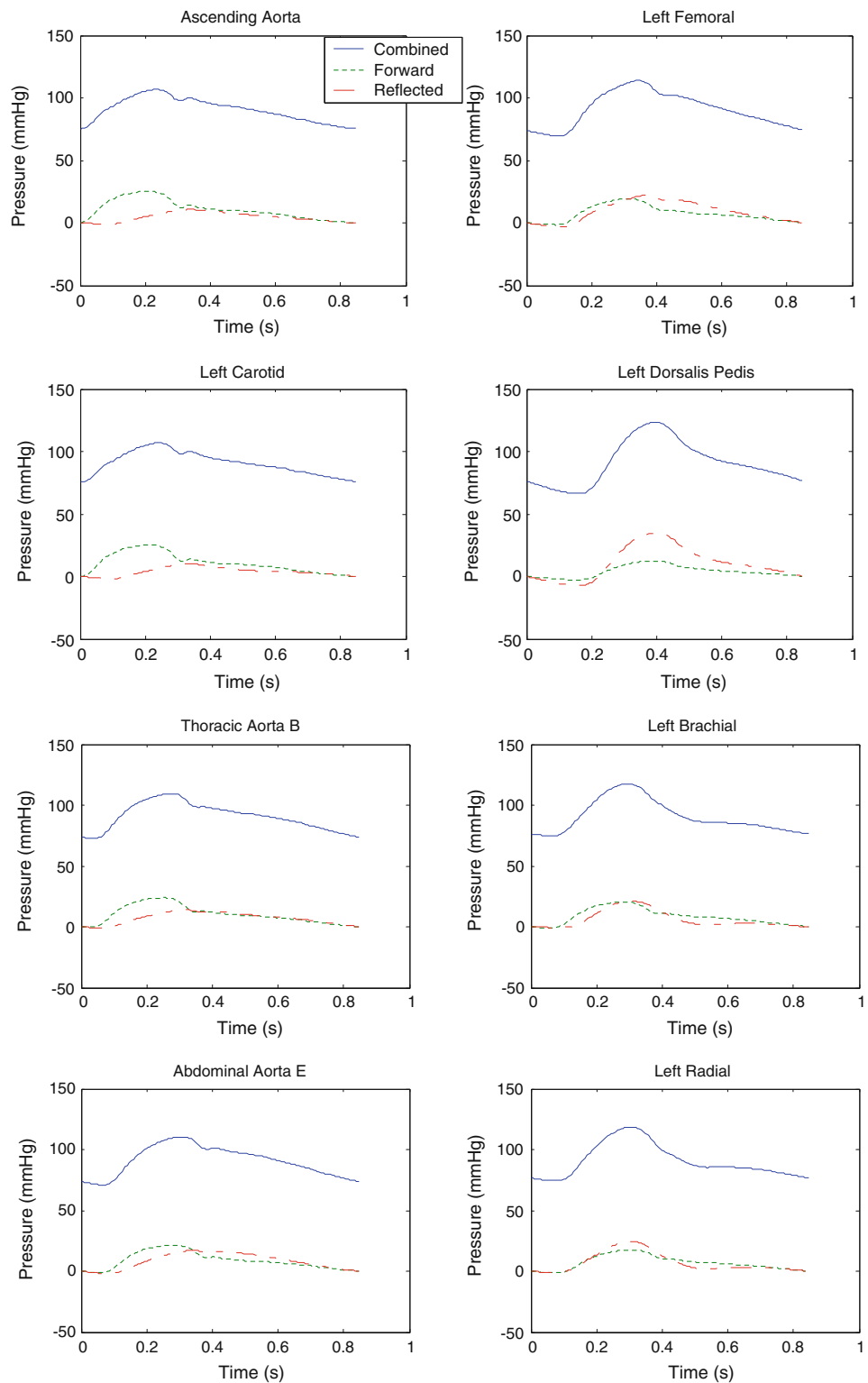
in the non-viscosity case. For the radial artery, the increase in the systolic peak, the amplified incisura and the second hump diastolic wave become more evident when compared with large elastic arteries. All these changes are due to less energy loss caused by wall viscosity.

Wall Elasticity

The pulse wave velocity c_0 changes with Young's modulus E as dictated by Moens-Korteweg equation, and therefore, the propagation constant γ, characteristic impedance Z_0,

Table 1 Hemodynamic parameters for the control conditions

	Dist. along aorta (cm)	SBP (mmHg)	DBP (mmHg)	PP (mmHg)	PPamp	PPF (mmHg)	PPFamp	PPR (mmHg)	PPRamp
Central									
Asc. aorta		106.80	75.21	31.58	1	25.22	1	11.61	1
L. Carotid	6	106.78	75.82	30.96	0.98	25.12	1.00	12.30	1.06
Th. Aorta B	25.5	109.59	72.50	37.09	1.17	24.15	0.96	15.28	1.32
Ab. aorta E	43.4	110.58	70.85	39.74	1.26	22.42	0.89	19.23	1.66
Lower limb									
Asc Aorta		106.80	75.21	31.58	1	25.22	1	11.61	1
L. femoral	64	113.81	69.40	44.41	1.41	20.61	0.82	25.35	2.18
L. dor. Ped	138.4	123.25	66.21	57.04	1.81	15.20	0.60	41.88	3.61
Upper limb									
Asc aorta		106.80	75.21	31.58	1	25.22	1	11.61	1
L. brachial	55.5	117.51	74.75	42.77	1.35	21.30	0.84	21.71	1.87
L. radial	79	118.53	74.38	44.15	1.40	18.56	0.74	25.60	2.20

SBP Systolic blood pressure, *DBP* diastolic blood pressure, *PP* pulse pressure, *PPamp* pulse pressure amplification against composite ascending aortic pressure, *PPF* pulse pressure of forward component, *PPFamp* amplification of forward pulse pressure against forward ascending aortic pressure, *PPR* pulse pressure of reflected component, *PPRamp* amplification of reflected pulse pressure against reflected ascending aortic pressure
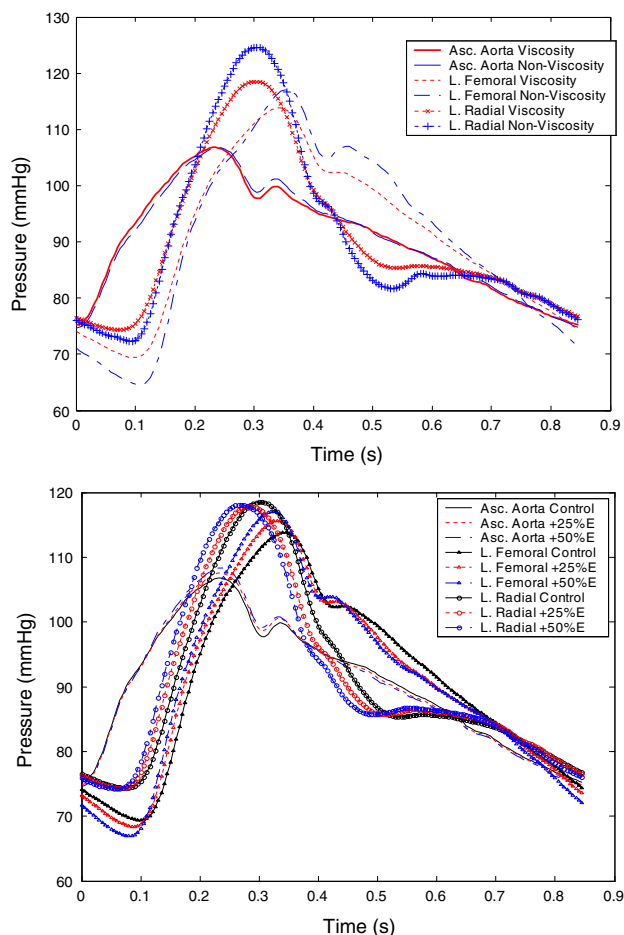

Fig. 4 Pressure waves for viscous versus non-viscous (*upper*) and for varying elastic moduli (*lower*)

and terminal reflection coefficient Γ_T all change with E accordingly. With increased E, the attenuation coefficient α decreases and the amplitude of the pressure wave increases; the phase coefficient β reflects the wave speed ($c_1 = \omega/\beta$, ω is the angular frequency) inversely, therefore the wave travels at a higher speed for higher E. In addition, the amplitude and speed of the traveling wave in a proximal artery become lower than those in a peripheral artery due to the higher E in the latter (elastic tapering). The terminal reflection coefficient decreases if E increases which tends to increase characteristic impedance. This, in turn, seemingly reduces the mismatch between the terminal impedance and the characteristic impedance. For 25 and 50% increased E, the computed pressure waveforms are shown in Fig 4 (lower).

The increase in elastic modulus shifts pressure waveforms in the ascending aorta and femoral artery to the upper left, and also make the second hump in the diastole more evident.

Discussions

In the present model the reflection is treated locally rather than globally based upon the intuitive thought that each traveling wave cannot predict what would happen beyond the point at the branch. This viewpoint agrees well with traditional transmission line models that reflections are treated globally with the global reflection as the summation of local reflections with minimal forward reflection. The model presented here is more flexible and provides a

causal-effect explanation of observed pressure waveforms in the central and peripheral arteries that the traditional transmission line models do not offer. The current model can find its use in deriving central pressure waveforms from peripheral non-invasive pressure measurements such as with an arterial tonometer.

Since the reflection and transmission patterns are solely dependent on the local characteristics, i.e. diameters, (this model is based upon one-dimensional linearized flow equations and the potentially important local factor—branch angle is ignored.) the zero forward reflection assumption becomes critical. From the current available data, most branches have very small local reflection coefficients that can be approximated as zero. But large reflections do occur at some major branches, such as in the thoracic aorta where the local forward reflection coefficient is about 40%. When this occurs, all the reflections from downstream will be greatly obscured.

The results of the sensitivity studies on the wall properties (elasticity and viscosity) are in good agreement with other investigators (Stergiopulos 1990; Karamanoglu et al. 1994, 1995; Segers et al. 1997). With appropriate manipulations of the terminal impedance (mainly resistance) and the wall elasticity, atherosclerosis and the effect of aging can be simulated.

Additional segments representing the limbs can add to a more faithful reproduction of the pressure waveforms in these regions. Using the original 121 segments by Westerhof et al. (1969) is also feasible. Obviously, with more segments, not only the reflection coefficients, but also the geometric and elastic tapering can be better represented. Another anticipated improvement of the model will be to include perfusion into certain organ vascular beds.

References

Avolio AP. Multi-branched model of the human arterial system. Med Biol Eng Comp. 1980;18:709–18. doi:10.1007/BF02441895.

Bergel DH. Dynamic elastic properties of the arterial wall. J Physiol. 1961;156:458–69.

Berger D, Li JK-J, Laskey WK, Noordergraaf A. Repeated reflection of waves in the systemic arterial system. Am J Physiol Heart & Circ Physiol. 1993;33(264):H269–81.

Gosling RG, Newman DL, Bowden NLR, Twinn KW. The are ratio of normal aortic junctions-aortic configuration and pulse wave reflection. Br J Radiol. 1971;44:850–3.

Guyton AC. Textbook of medical physiology. 5th ed. Philadelphia: Saunders; 1976.

Hardung V. Uber eine Methode zur Messung der dynamischen Elastiziat und Viskositat kautschukahnlicher Korper, insbesondere von Blutgefassen und anderen elastischen Gewebteilen. Helv Physiol Acta. 1952;10:482–98.

Karamanoglu M, Gallagher DE, Avolio AP, O'Rourke MF. Functional origin of reflected pressure waves in a multibranched model of the human arterial system. Am J Physiol. 1995;267:H1363–9.

Karamanoglu M, Gallagher DE, Avolio AP, O'Rourke MF. Pressure wave propagation in a multibranched model of the human upper limb. Am J Physiol. 1994;269:H1681–8.

Li JK-J, Melbin J, Noordergraaf A. Directional disparity of pulse wave reflections in dog arteries. Am J Physiol Heart & Cir Physiol. 1984;247:H95–9.

Li JK-J. Time domain resolution of forward and reflected waves in the aorta. IEEE Trans Biomed Eng. 1986a;BME-33:783–5. doi:10.1109/TBME.1986.325903.

Li JK-J. Dominance of geometric over elastic factors in pulse transmission through arterial branching. Bull Math Biol. 1986b;48:97–103.

Li JK-J. Arterial systems dynamics. New York: New York Univerity Press; 1987.

Li JK-J. Increased arterial pulse wave reflections and pulsatile energy loss in acute hypertension. Angiology J Vasc Dis. 1989;40:730–5.

Li JK-J. The arterial circulation: physical principles and clinical applications. Totowa, NJ: Humana Press; 2000.

Li JK-J. Dynamics of the vascular system. Singapore: World Scientific Publishers; 2004.

Li JK-J, Zhu Y, O'Hara D, Khaw K. Allometric hemodynamic analysis of isolated systolic hypertension and aging. Cardiovasc Eng. 2007;7:135–9. doi:10.1007/s10558-007-9040-x.

McDonald DA. Blood flow in arteries. 2nd ed. London: Edward Arnold Ltd; 1974.

O'Rourke MF. Arterial hemodynamics in hypertension. Circ Res. 1970;27(2):123–33.

Papageorgiou GL, Jones NB, Redding VJ, Hudson N. The area ratio of normal arterial junctions and its implications in pulse wave reflections. Cardiovasc Res. 1990;6:478–84. doi:10.1093/cvr/24.6.478.

Noordergraaf A, Jager GN, Westerhof N, editors. Circulatory analog computers, Proc. of symposium on development of analog computers in the study of mammalian circulatory systems. Amsterdam: North-Holland Publishing; 1963.

Noordergraaf A. Hemodynamics. In: Schwann HP, editor. Biological Engineering. New York: McGraw-Hill; 1969.

Safar ME, Simon AC, Levenson JA. Structural changes of large arteries in sustained essential hypertension. Hypertension. 1984;6(3):117–21.

Schaaf BW, Abbrecht PH. Digital computer simulation of human systemic arterial pulse transmission: a non-linear model. J Biomech. 1972;5:345–64.

Segers P, Stergiopulos N, Verdonck P, Verhoeven R. Assessment of distributed arterial network models. Med Biol Eng Comput. 1997;35:729–36.

Snyder MF, Rideout VC, Hillestead RJ. Computer modeling of the human systemic arterial tree. J Biomech. 1968;1:341–53.

Stergiopulos N. Computer simulation of arterial blood flow. Ph.D. Dissertation. Iowa State University, Ames; 1990.

Stergiopulos N, Young DF, Rogge TR. Computer simulation of arterial flow with applications to arterial and aortic stenoses. J Biomech. 1992;25(12):1477–88.

Taylor MG. Wave transmission through an assembly of randomly branching elastic tubes. Biophys J. 1966;6(6):697–716.

Wang JJ. Wave Propagation in a model of the human arterial system. Ph.D. Dissertation. University of London, London; 1997.

Wang JJ, Parker KH. Wave propagation in a model of the arterial circulation. Biomechanics. 2004;37:457–70.

Westerhof N, Bosman F, DeVries CJ, Noordergraaf A. Analog studies of the human systemic arterial tree. J Biomech. 1969;2:121–43.

Womersley JR. Oscillatory flow in arteries: the constrained elastic tube as a model of arterial flow and pulse transmission. Phys Med Biol. 1957;2(2):178–87.

Zhang H. A novel frequency domain arterial tree model: distributed wave reflections and potential clinical applications. Ph.D. Dissertation. Rutgers, the State University of New Jersey; 2006.